Estimating River Surface Elevation From ArcticDEM

Chunli Dai[1] [iD], **Michael Durand[2]** [iD], **Ian M. Howat[2]** [iD], **Elizabeth H. Altenau[3]** [iD], and **Tamlin M. Pavelsky[3]** [iD]

[1]School of Earth Sciences, The Ohio State University, Columbus, OH, USA, [2]School of Earth Sciences and Byrd Polar Research Center, The Ohio State University, Columbus, OH, USA, [3]Department of Geological Sciences, University of Chapel Hill, Chapel Hill, NC, USA

Abstract ArcticDEM is a collection of 2-m resolution, repeat digital surface models created from stereoscopic satellite imagery. To demonstrate the potential of ArcticDEM for measuring river stages and discharges, we estimate river surface heights along a reach of Tanana River near Fairbanks, Alaska, by the precise detection of river shorelines and mapping of shorelines to land surface elevation. The river height profiles over a 15-km reach agree with in situ measurements to a standard deviation less than 30 cm. The time series of ArcticDEM-derived river heights agree with the U.S. Geological Survey gage measurements with a standard deviation of 32 cm. Using the rating curve for that gage, we obtain discharges with a validation accuracy (root-mean-square error) of 234 m³/s (23% of the mean discharge). Our results demonstrate that ArcticDEM can accurately measure spatial and temporal variations of river surfaces, providing a new and powerful data set for hydrologic analysis.

Plain Language Summary Arctic rivers are poorly observed despite their potential sensitivity to climate change and importance to global hydrology. This is due to the sparsity of gages and lack of a reliable space-based method for measuring river stage and discharge. Here we demonstrate that ArcticDEM, a collection of openly available repeat Digital Surface Models derived from submeter resolution satellite imagery, provides a powerful new data source for measuring river surface elevations and discharge from space. We apply these data near the Tanana River, Alaska, and compare ArcticDEM results to airborne and ground observations finding that ArcticDEM is able to detect short-term variability in river height. Thus, ArcticDEM enables remote sensing measurements of currently unobserved rivers, improving our understanding of Arctic hydrology.

1. Introduction

Improving knowledge of Arctic rivers is of utmost importance; rivers integrate climate and surface processes and serve as indicators of change. While the total river discharge into the global Arctic Ocean is relatively well-constrained (Peterson, 2002; Steele et al., 1996), the size of these basins (millions of km²) convolves countless processes, obscuring the causes of change. Smaller tributaries in the Arctic, including North America, are some of the least-well-gaged rivers in the world, and many of these rivers are braided. However, a framework for remote sensing of river discharge in ungaged, braided rivers does not yet exist, in the absence of in situ calibration data.

While no remote sensing technique, as yet, can directly measure river discharge, multiple methods exist for estimating discharge from observed river height, width, and slope (e.g., Bjerklie et al., 2005; Durand et al., 2016; Gleason & Smith, 2014). River surface heights and slopes can be measured directly from radar altimetry (e.g., Birkett et al., 2002; Frappart et al., 2006; Papa et al., 2012) or may be obtained by mapping shorelines into precise digital surface models (DSMs, e.g., Hostache et al., 2009; Schumann et al., 2007; Tseng et al., 2016). While the former method is a primary measurement objective of NASA's Surface Water and Ocean Topography (SWOT) mission (Biancamaria et al., 2016), scheduled for 2021, current spaceborne radar altimeters are only capable of reliably measuring surface heights of rivers with widths of at least a few kilometers (Papa et al., 2012). The SWOT Ka-band radar interferometer instrument will be capable of measuring rivers wider than 50 to 100 m (Pavelsky et al., 2014). Imagery-based methods, such as presented in this study, provide relatively high spatial resolution (~20 m width). Nevertheless, the use of imagery is limited by cloud cover and light conditions which reduce the quality and temporal resolution of measurements. Further, DSM coverage of the Arctic with a spatial resolution and accuracy sufficient for measuring river heights from shorelines has, until recently, been limited to sparse LiDAR surveys.

ArcticDEM (Morin et al., 2016, http://arcticdem.org) is a collection of high-resolution (2 m) DSMs of the Arctic, created from 0.32 to 0.5 m resolution, panchromatic-band stereoscopic satellite imagery acquired by the DigitalGlobe constellation of optical imagers: WorldView-1 (2007), WorldView-2 (2009), WorldView-3 (2014), and GeoEye-1 (2008). While these sensors, with the exception of WorldView-1, also acquire imagery in the multispectral bands, panchromatic bands are used for DSM creation due to their higher ground sample resolution. We note that ArcticDEM provides the elevation of vegetation and man-made structures, which defines a DSM, rather than that of bare-Earth, which usually defines a digital elevation model (DEM). ArcticDEM encompasses all land area north of 60°N, as well as all territory of Greenland, the State of Alaska in entirety, and the Kamchatka Peninsula of the Russian Federation. ArcticDEM's wide area of repeated coverage and high spatial resolution offer an unprecedented new data set for observing river hydrology. While stereo-photogrammetry cannot measure water surface height directly, ArcticDEM provides simultaneous land surface elevation and imagery at high resolution, offering the potential for concurrent mapping of shoreline location and elevation to decimeter precision. Further, multiple DSMs are obtained, with some areas having over 10 repeats per year, enabling change measurement at seasonal to interannual timescales.

To test the potential for ArcticDEM measurements of river discharge, we apply automated shoreline mapping and height retrieval algorithms to a gaged reach of the Tanana River, Alaska, and compare our river height retrievals to those obtained from multiple, independent, high-precision sources. Finally, we assess the impact of uncertainty in ArcticDEM-derived river heights on rating-curve discharge estimates and comparison to gage data.

2. Data and Methods

2.1. ArcticDEM DSMs and Orthoimagery

ArcticDEM DSMs and orthorectified imagery are generated using the Surface Extraction from TIN-based Searchspace Minimization stereo-photogrammetry software (Noh & Howat, 2015, 2017). The DSMs are created by collocating pixels between pairs of overlapping imagery with known camera orientation and imaging geometry. The offsets of the collocated points in pixel coordinates yield a parallax field that is then converted into elevation of the imaged surface. The archive of DSMs since 2007 is publicly available at the ArcticDEM website maintained by the Polar Geospatial Center. The products include individual DSM strips (i.e., collected along a satellite single pass) at 2-m spatial resolution and typically 17 km in width 110 km in length (Morin et al., 2016). Each panchromatic band image pair used for DSM extraction is orthorectified and is available to U.S. federally funded investigators.

While DSMs have an internal (pixel-to-pixel) accuracy of 0.2 m (Noh & Howat, 2015), the initial geolocation may have systematic offsets of 3–5 m in the vertical and horizontal resulting from errors in the sensor model that relates the image pixel coordinates to map coordinates. These biases may be removed with a single control point, such as from a ground Global Positioning System (GPS) survey point or lidar transect, or by coregistration to a reference DSM for change measurement. We coregister sets of DSMs using the three-dimensional fitting method of Nuth and Kääb (2011), in which the vertical offset and the spatial trend in aspect are iteratively removed.

2.2. River Classification and Shoreline Mapping

Our approach to deriving river surface height from ArcticDEM requires (1) accurately detecting the river shoreline and (2) co-locating shoreline points with the appropriate land surface elevation. Existing river maps derived from Landsat (e.g., Du et al., 2012; Ottinger et al., 2013) are of much coarser resolution (30 m) than ArcticDEM (2 m) and for large rivers (60–100 m wide); hence, they do not account for changes in river width through time for most gaged rivers in the Arctic, including our study area. Previous analysis of 5-m resolution RapidEye imagery over our Tanana River study reach suggests that its width variability is detectable from satellite imagery and that width variations are strongly predictive of discharge (Pavelsky, 2014).

Since only the orthorectified panchromatic (pan) band source imagery is produced through ArcticDEM, and WorldView-1 only collects a pan band, we seek an automated river surface classification algorithm that uses the pan band texture and brightness rather than the widely used two-band Normalized Difference Water Index method (McFeeters, 1996). Our approach combines image entropy and brightness thresholding. An entropy-based method has been used for identifying large water bodies, for example, lakes or large rivers

(>500 m width) from pan band imagery (Mohamed & Kim, 2003; Zhaohui et al., 2003). A brightness threshold method for panchromatic or single-band imagery has also been proposed for land cover classification (e.g., Frazier & Page, 2000; Hamandawana et al., 2006; Zhao et al., 2011). While, in these applications, brightness threshold values are obtained from analysis of known water surfaces, we require a method in which no a priori knowledge of the location of water is required. Thus, we combine the entropy and brightness thresholding classification methods to delineate shorelines of narrow rivers from high resolution (2 m) panchromatic imagery. The entropy H at a pixel in one image is defined as (Zhaohui et al., 2003)

$$H = -\sum_{i=1}^{J} p_i \log_2(p_i)$$

where J is the total number of gray level values within a 5×5 kernel of neighboring pixels centered on the target pixel and p_i is the probability that each pixel will be of gray scale level i, calculated from the histogram of all gray level values within the kernel. The water surface typically has lower entropy than the land surface, as well as a uniform panchromatic reflectance. Therefore, our approach assumes that the combination of uniform radiance and low entropy can uniquely define river channels. We first retrieve an initial mask of water surface based on solely the entropy threshold. Since the majority of pixels within the mask are water surface, the mean and standard deviation of their brightness represent the water surface reflectance. We thus refine the entropy-based classification by classifying all pixels whose brightness is within one standard deviation of this mean.

Taking an image over a reach of the Tanana River, Alaska, as an example, the smooth texture of water surfaces in the panchromatic orthoimage (Figure 1a) yields relatively low entropy (Figure 1b) compared to land surfaces. A threshold applied to the entropy image provides a rough river mask (Figure S1a in the supporting information), but with some misclassification and blurring of the shoreline resulting from the 5×5 pixel neighborhood used to calculate entropy. We obtain an improved classification through application of the brightness threshold determined from the statistics of the entropy-classified pixels. This yields the river water surface mask (Figure 1c), which we validate though comparison to a mask obtained from the Normalized Difference Water Index method applied to the multispectral bands of the same GeoEye-1 image (Figure S1b). We find the water mask areas determined by two methods agree within 0.8% (Figure S1b), which demonstrates the viability of the proposed entropy/brightness method (see Figure S1) when only panchromatic band imagery is available. The shorelines are then obtained from the mask boundaries using a morphological filter (Figure 1d). This method successfully detects river widths as narrow as 20 m from WorldView imagery.

2.3. River Height and Slope Extraction and Validation

Once the river shoreline is mapped, shoreline elevation pixels can either be directly extracted from the DSM or derived using the imagery-altimetry method (e.g., Durand et al., 2014; Tseng et al., 2016) that uses the lowest-stage reference DSM with time-variable shorelines. The imagery-altimetry method has the advantage that once a single, lowest-stage reference DSM is available, only the repeat imagery, and not DSMs, is required to estimate river height. Since both methods are possible with ArcticDEM, we apply and compare both approaches with the expectation that the preferred method for a particular site likely depends on river morphology and data availability. Both methods require subpixel image and DSM coregistration (with the same correction applied to the corresponding orthoimagery) (Nuth & Kääb, 2011), or 2-D feature matching in the case where only imagery are used.

Using either approach, extracted shoreline DSM pixels are mapped onto the nearest point or "node" along the main channel centerline. In order to focus on shoreline mapping, height extraction, and discharge estimation in this study, centerlines for multichannel rivers are drawn manually for one main channel. In our test applications, we have found that the distribution of heights within a given node is often strongly skewed (Figure S2). The "long tail" contains heights contaminated by nonshoreline features, whereas the lower quantiles of the data accurately reflect river elevations. We then use the following heuristic approach to retrieve water surface profiles and slopes from the DSMs: (1) A preliminary elevation is assigned to each node (spaced at 100 m along centerline), based on the 25th percentile of associated pixel elevations. If there are fewer than 20 pixels or the standard deviation exceeds 250 cm, that node is not used in subsequent processing. (2) For each DSM, a preliminary, monotonic-decreasing water surface profile along the centerline is computed to
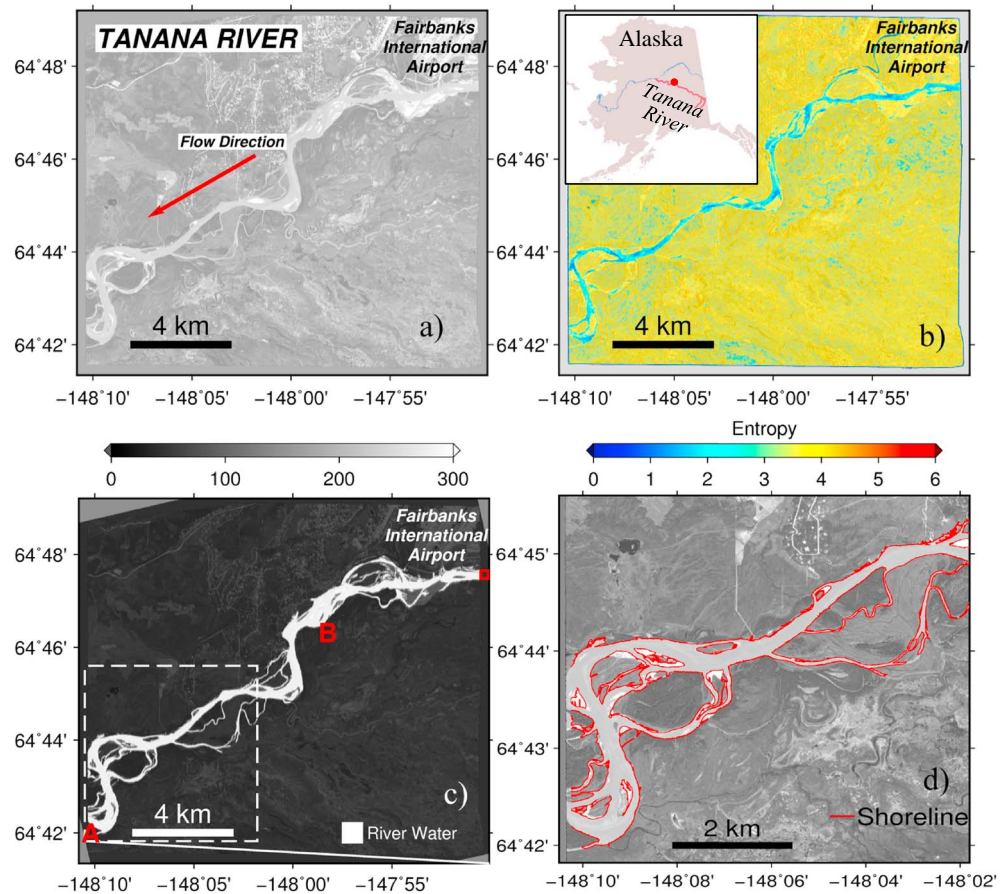
Figure 1. Example of river classification and shoreline mapping. (a) Orthorectified GEOEYE-1 image for a section of the Tanana River, Alaska, on 26 May 2013. The color bar shows gray scale brightness (unitless digital number). (b) Local entropy (unitless) of the image shown in (a); note that the entropy of the water surface is low. (c) Binary water mask where water equals one (white area) and all land pixels equal zero (nonwhite area). The transparent background is the gray scale image. The red square denotes the Fairbanks U.S. Geological Survey gage, and "AB" is the profile shown in Figure 2a. (d) The detected river shoreline (red) for the selected region (white box in (c)). Imagery© 2013 DigitalGlobe, Inc.

minimize the L-1 norm (least absolute deviation) of the profile versus node residuals. (3) A final elevation is assigned to each node using the parameters described in step 1, but excluding all pixels >100 cm from the preliminary water surface profile (computed in step 2). (4) A final water surface profile is computed by fitting a monotonic-decreasing cubic function to the final node elevations. The cubic function is differentiated to obtain spatially continuous river slope. The code for retrieving and filtering river heights from ArcticDEM data is available at Github (https://github.com/Chunli-Dai/RiverHeights and https://github.com/mikedurand/SmoothRiverElevations).

2.4. Error Sources

Assuming clear-sky imagery, a high Sun-angle, and standard stereoscopic view angles, uncertainty in river height change measurements is due to (1) random DSM internal (pixel-to-pixel) height errors, (2) pixel resolution, (3) coregistration errors, and (4) errors in shoreline location. Source (1) imparts a standard error of 20 cm (Noh & Howat, 2015), while (2) varies with pixel resolution, r, and river bank slope, ?, as $r\tan(?)$, or 39 cm for a 2-m resolution DSM/orthoimage and a 11° slope, which is the average bank slope (standard deviation, 10°) for a 10 km reach in Figure 1a. Error sources (1) and (2) are expected to be correlated over relatively short spatial scales and will, therefore, have a small impact on river heights at the scale of hundreds of meters through filtering and smoothing. Since river surfaces are relatively flat at the scale of a reach, filtering and smoothing along a reach largely mitigates the random DSM errors. Thus, the combined error from sources (1) and (2) is expected to be approximately 10 cm. Source (3) is the largest potential error source and is
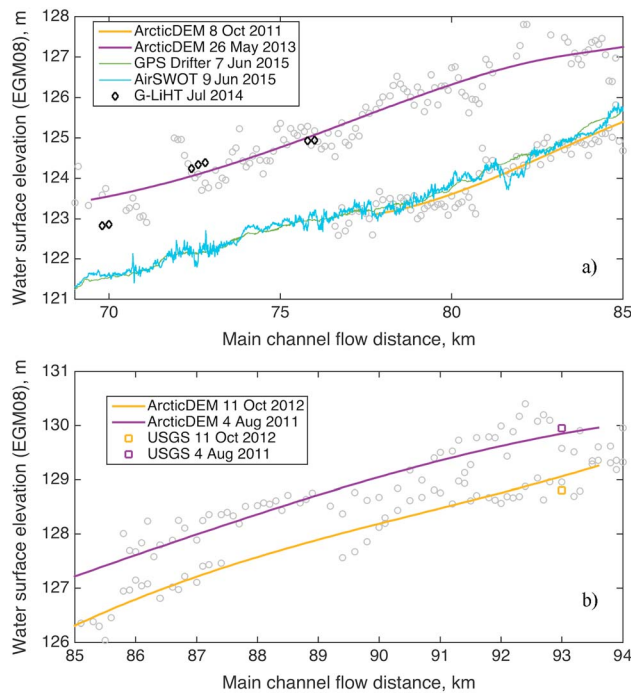
Figure 2. River water surface elevations extracted from ArcticDEM on the Tanana River compared with Global Positioning System (GPS) drifter, AirSWOT, G-LiHT, and an in situ gage, with respect to flow distance upstream of Nenana. The GPS drifter observations acquired on 7 June are adjusted by the average stage difference (−17.8 cm; Altenau et al., 2017) to compare to 9 June AirSWOT measurements. (a) The water surface elevations along the profile "AB" in Figure 1 and (b) along profile from point B to the U.S. Geological Survey gage (Figure 1). The gray circles throughout are ArcticDEM elevations averaged to 100-m resolution along centerline. In (b), the average difference between the gage and ArcticDEM (around 1 m) was removed in order to emphasize temporal stage change.

systematic. Coregistration errors most commonly result from misapplication of ground control (i.e., surfaces assumed fixed in space were not), artifacts in the DSM, and subpixel ambiguity in the ICP solution. Here, they are evaluated from coregistration residuals over control surfaces, whose standard deviation is around 60 cm for each pair of DSMs. The stability of the solution is also assessed by repeating coregistration for multiple subsets of the DSM/orthoimage. The direct method of extracting river heights is only affected by vertical translation, whereas the imagery-altimetry method is only affected by the horizontal translational parameters. Thus, for the imagery-altimetry method, errors due to horizontal coregistration decrease with river bank slope. Error source (4), resulting from errors in shoreline location, is expected to be small relative to error sources (1)–(3) due to the filtering and averaging within the river height extraction approach described in section 2.3.

2.5. Validation Data Sets

We validate measurements obtained from ArcticDEM through comparison to four independent data sets. First, we use airborne, multibaseline Ka-band InSAR altimetry obtained with the AirSWOT instrument on 9 June 2015 over the Tanana River. AirSWOT elevation data, processed and distributed by NASA Jet Propulsion Laboratory, have a spatial resolution of 3.6 m and an uncertainty of 9 cm after filtering and smoothing (Altenau et al., 2017). Second, we use airborne LiDAR altimetry obtained in July 2014 with the NASA G-LiHT system (Cook et al., 2013) (https://glihtdata.gsfc.nasa.gov). G-LiHT footprints have a typical footprint size and vertical accuracy of 10 cm (Cook et al., 2013). Third, we use elevation and position measurements obtained from a boat-mounted Global Positioning System (GPS Drifter) on 7 June 2015. The water surface elevation profile was measured nearly continuously (0.5-s intervals; ~3 m spacing) using a Trimble R9 survey-grade GPS system along the main channel of the river. Total uncertainty for the GPS profile is around 9.9 cm (Altenau et al., 2017). Finally, we use height and discharge data from USGS gage station 15485500 in Fairbanks, AK.

The accuracy of height is about 3 mm. Based on the stage-discharge rating curve, the discharge precision at the gauge is estimated to be around 45 m³/s (~4% of mean discharge) from posteriori variance of unit weight (Cohn et al., 2013; Harmel et al., 2006). Data are processed and provided by the USGS's National Water Information System (https://nwis.waterdata.usgs.gov/nwis/sw, last accessed October 2017). Two tributaries enter the Tanana within our study area: the Chena River (which is gaged) and Salchacket Slough (which is not); together these represent <20% of Tanana River discharge during ordinary conditions. To avoid complications related to tributary junctions, we compare the time series of ArcticDEM river elevations to USGS gaged elevations and streamflow only in the immediate vicinity of the gage.

3. Results

Results for the Tanana River test site, obtained using the procedures described above, are shown in Figure 2, along with the validation data sets. Figure 2a shows the river surface elevation profile between Byers and Sam Charley Islands downstream of Fairbanks (between points A and B in Figure 1). We find that the direct and imagery-altimetry methods provide consistent estimates of unfrozen river height (Figure S3) with a standard deviation of only 0.26 m between two methods. For clarity, Figure 2 shows only the ArcticDEM heights obtained using the imagery-altimetry method with a lowest-stage reference DSM from 8 October 2011. Note that streamflow at the closest USGS gage was around 440 m³/s on 8 October 2011 and 1,060 m³/s on 26 May 2013, corresponding to the lower and higher water surface elevation profiles, respectively. Similar spatial patterns are evident between data sets, however, with ArcticDEM showing similar slopes as both the in situ (GPS drifter) and airborne data (G-LiHT and AirSWOT). The respective standard deviations
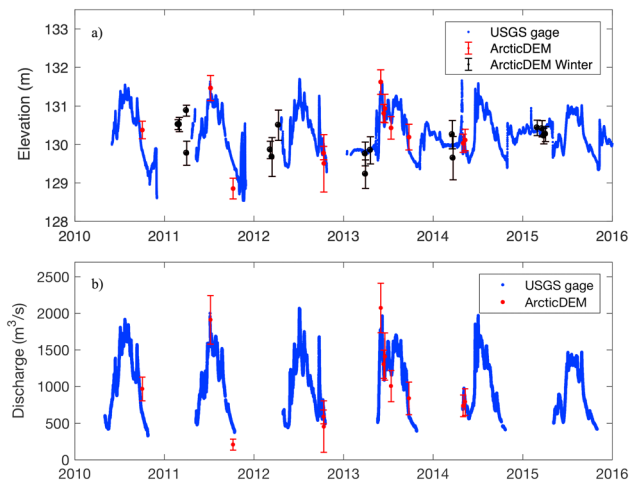
Figure 3. Time series of river height and discharge at the U.S. Geological Survey (USGS) gage at Tanana River, Fairbanks, Alaska. (a) The blue dots are the in situ gage height data. The red dots are the river heights estimated from ArcticDEM (direct method) averaged along 1 km reach near the gage, and the error bar is the estimated uncertainty, which is around 0.3 m. The black dots are ArcticDEM river heights in winter season (November to April). For each ArcticDEM measurement, the coregistration uncertainty with respect to the reference digital surface model (DSM) is around 0.6 m, which is the standard deviation of height differences between two DSMs over control surfaces. The average difference between the gage and ArcticDEM was removed in order to emphasize temporal stage change. (b) Discharge time series from USGS (blue) and ArcticDEM (red). The standard deviation of the ArcticDEM discharge based on error propagation from river height uncertainty is around 219 m^3/s.

of the height differences between May 2013 ArcticDEM and the GPS, G-LiHT, and AirSWOT were 24, 29, and 28 cm, where the mean height differences (biases) were removed prior to the computation of standard deviations. For 8 October 2011 and 26 May 2013, the ArcticDEM slope errors compared to the GPS drifter were 1.5 and 0.2 cm/km, respectively. Slopes were evaluated from 77 to 85 km and from 70 to 85 km for 8 October 2011 and 26 May 2013, respectively.

Figure 2b shows results upstream and including the USGS gage at Fairbanks. Note that most USGS gage datums are not known to within high precision, so the average difference between the gage and ArcticDEM (~1 m) was removed for this comparison, in order to focus on comparing stage change between two passes. The difference might be caused by the accuracy of the reference vertical datum of the gage or that of the ArcticDEM elevation. The change in elevation between passes is 110 cm at the gage and 70 cm from ArcticDEM final water surface profiles. The deviations of ArcticDEM residuals from the fitted surfaces were 29, 43, 42, and 26 cm for the October 2011, May 2013, August 2011, and October 2012 DSMs.

There are about 30 ArcticDEM DSMs (Table S1 in the supporting information) acquired at different times covering the USGS gage at Fairbanks, each providing a river height profile similar to that shown in Figure 2. Half of the DSMs were acquired in winter, when ice and snow cover prevent an entropy-based water surface classification. For wintertime DSMs, since ice and snow provide reliable surface elevations in the DSM, we instead retrieve heights along the surface within 20 m of the river centerline. This provides a river height that might be overestimated by an unknown amount due to the thickness of the ice and snow cover, which we assess through comparison with the gage estimates. For all measurements, the river height at the gage is calculated by the average value of river heights along a 1 km reach near the gage. The time series of river heights at the gage are then compared with the in situ gage data (Figure 3a). The average difference between the gage and ArcticDEM was removed due to the uncertainties in the gage's vertical datum as describe above. The ArcticDEM river height estimates have a 1-sigma uncertainty of around 30 cm, and the difference between ArcticDEM estimates and concurrent gage measurements gives a standard deviation of 32 cm.

We estimate discharge from the time series of ArcticDEM-derived water surface heights using the empirical stage-discharge rating curve approach (e.g., Papa et al., 2012). The rating curve was obtained from fitting a second order polynomial to USGS gage height and discharge data between 2010 and 2016 (Figure S4). It is worth mentioning that since the ArcticDEM river elevations are measured in the immediate vicinity (1 km) of the USGS gage, our estimated discharges only represent the streamflow at the USGS gage. We also estimate the formal uncertainty of discharge through error propagation, which is shown in Figure 3b and Figure S4. The root-mean-square error (RMSE) of ArcticDEM discharges with respect to the USGS gage discharge is 234 m^3/s (Figure S5) or ~23% of the mean discharge (1,027 m^3/s) between 2010 and 2016. Here the mean difference (bias) of 72 m^3/s is included in the calculation of RMSE. This discharge RMSE is slightly larger than that (~6%) estimated from width variations measured by RapidEye satellite imagery based on width-discharge relationship (Pavelsky, 2014).

4. Discussion and Conclusion

ArcticDEM provides a new, year-round data source for measuring river surface heights, as well as river slopes and discharges. Results from ArcticDEM are compared with in situ measurements of river height, demonstrating spatial and temporal resolutions. The precision of ArcticDEM water height is around 30 cm both from the water surface elevation (averaged over a 1 km reach) time series and from a long (15 km) reach of river profile, which is comparable to the accuracy goal (10 cm over 1 km^2 area) of SWOT (Pavelsky et al., 2014). We note that this precision is dependent on the spacing of profile nodes (see section 2.3), for which we use 100 m.

Increasing the node spacing to 200 m, as expected for SWOT, would further improve precision at the expense of spatial resolution. Heights obtained directly from the frozen river surface in winter have similar uncertainties as shoreline-derived estimates and no systematic bias when compared to gage measurements, suggesting that wintertime estimates are also possible. The lack of a bias resulting from ice and snow cover may be due to a similar thickness of snow cover on the control surface used for coregistration, so that a systematic height bias of that thickness would be consistent over the DSM and would, therefore, cancel out when measuring river surface height change.

Along a 15-km reach, the difference between slopes measured from ArcticDEM and the GPS Drifter is less than 1.5 cm/km. Using the empirical stage-discharge relationship, the river discharge time series is derived from ArcticDEM water surface elevation estimates, yielding an accuracy of 234 m^3/s (23% of the mean discharge) when compared to in situ data. Measurements of river geometry (height, width, and slope) and use of the Manning equation and Mass-Conserved Flow Law Inversion algorithms (Durand et al., 2010, 2014, 2016) may enable discharge estimates for ungaged rivers from ArcticDEM. This work lays the groundwork for remote sensing of river dynamics and discharge estimates in ungaged basins for braided rivers over entire Arctic with ArcticDEM.

One critical factor that makes this method of measuring river heights using ArcticDEM successful is the fact that river surfaces are fairly flat over local scales, so that the filtering and averaging along a section of river (e.g., 1 km reach) can largely mitigate the random errors in DSMs. We successfully apply a river classification method based on panchromatic band entropy and brightness to a braided river with high silt content, which are typically challenging characteristics for river mapping. Our method for measuring river heights, however, requires that that river surface area varies detectably with water surface elevation, and so may be less applicable to rivers tightly constrained by levees, bluffs, and other steep bank forms. Further testing is also needed to constrain the uncertainty associated with this approach, including the minimum resolvable channel width, and its dependence on sensor geometry, ice cover, settings, and light conditions.

Further work can be carried out to provide critical measurements (river height, width, and slope over long river reaches) for validating Manning equation and Mass-Conserved Flow Law Inversion algorithms for the upcoming SWOT mission and will inform the theoretical basis for choice of SWOT discharge algorithms, especially for braided rivers. In addition, a database of land/water masks can be generated to help refine the SWOT target regions, and the assignment of water surface elevation from the shoreline to the main channel can be used for training SWOT water surface elevation extraction algorithms, as well as smoothing and filtering algorithms. ArcticDEM and SWOT data can be integrated for rivers covered by both measurements. Due to their complementary properties, water elevations, and river discharge extracted from submeter, stereoscopic satellite imagery may provide an indispensable new global data stream that can complement SWOT in coming years.

References

Altenau, E. H., Pavelsky, T. M., Moller, D., Lion, C., Pitcher, L. H., Allen, G. H., et al. (2017). AirSWOT measurements of river water surface elevation and slope: Tanana River, AK. *Geophysical Research Letters*, 44, 181–189. https://doi.org/10.1002/2016GL071577

Biancamaria, S., Lettenmaier, D. P., & Pavelsky, T. M. (2016). The SWOT mission and its capabilities for land hydrology. *Surveys in Geophysics*, 37(2), 307–337. https://doi.org/10.1007/s10712-015-9346-y

Birkett, C. M., Mertes, L. A. K., Dunne, T., Costa, M. H., & Jasinski, M. J. (2002). Surface water dynamics in the Amazon Basin: Application of satellite radar altimetry. *Journal of Geophysical Research*, 107(D20), 8059. https://doi.org/10.1029/2001JD000609

Bjerklie, D. M., Moller, D., Smith, L. C., & Dingman, S. L. (2005). Estimating discharge in rivers using remotely sensed hydraulic information. *Journal of Hydrology*, 309(1–4), 191–209. https://doi.org/10.1016/j.jhydrol.2004.11.022

Cohn, T. A., Kiang, J. E., & Mason, R. R. Jr. (2013). Estimating discharge measurement uncertainty using the interpolated variance estimator. *Journal of Hydraulic Engineering*, 139(5), 502–510. https://doi.org/10.1061/(ASCE)HY.1943-7900.0000695

Cook, B. D., Nelson, R. F., Middleton, E. M., Morton, D. C., McCorkel, J. T., Masek, J. G., et al. (2013). NASA Goddard's LiDAR, hyperspectral and thermal (G-LiHT) airborne imager. *Remote Sensing*, 5(8), 4045–4066. https://doi.org/10.3390/rs5084045

Du, Z., Linghu, B., Ling, F., Li, W., Tian, W., Wang, H., et al. (2012). Estimating surface water area changes using time-series Landsat data in the Qingjiang River basin, China. *Journal of Applied Remote Sensing*, 6(1), 063609. https://doi.org/10.1117/1.JRS.6.063609

Durand, M., Gleason, C. J., Garambois, P. A., Bjerklie, D., Smith, L. C., Roux, H., et al. (2016). An intercomparison of remote sensing river discharge estimation algorithms from measurements of river height, width, and slope. *Water Resources Research*, 52, 4527–4549. https://doi.org/10.1002/2015WR018434

Durand, M., Neal, J., Rodríguez, E., Andreadis, K. M., Smith, L. C., & Yoon, Y. (2014). Estimating reach-averaged discharge for the river Severn from measurements of river water surface elevation and slope. *Journal of Hydrology*, 511, 92–104. https://doi.org/10.1016/j.jhydrol.2013.12.050

Durand, M., Rodriguez, E., Alsdorf, D. E., & Trigg, M. (2010). Estimating river depth from remote sensing swath interferometry measurements of river height, slope, and width. *IEEE Journal of Selected Topics in Applied Earth Observations and Remote Sensing*, 3(1), 20–31. https://doi.org/10.1109/JSTARS.2009.2033453

Frappart, F., Calmant, S., Cauhopé, M., Seyler, F., & Cazenave, A. (2006). Preliminary results of ENVISAT RA-2-derived water levels validation over the Amazon basin. *Remote Sensing of Environment*, *100*(2), 252–264. https://doi.org/10.1016/j.rse.2005.10.027

Frazier, P. S., & Page, K. J. (2000). Water body detection and delineation with Landsat TM data. *Photogrammetric Engineering and Remote Sensing*, *66*(12), 1461–1468.

Gleason, C. J., & Smith, L. C. (2014). Toward global mapping of river discharge using satellite images and at-many-stations hydraulic geometry. *Proceedings of the National Academy of Sciences of the United States of America*, *111*(13), 4788–4791. https://doi.org/10.1073/pnas.1317606111

Hamandawana, H., Eckardt, F., & Ringrose, S. (2006). The use of step-wise density slicing in classifying high-resolution panchromatic photographs. *International Journal of Remote Sensing*, *27*(21), 4923–4942. https://doi.org/10.1080/01431160600857436

Harmel, R. D., Cooper, R. J., Slade, R. M., Haney, R. L., & Arnold, J. G. (2006). Cumulative uncertainty in measured streamflow and water quality data for small watersheds. *Transactions of the ASABE*, *49*(3), 689–701. https://doi.org/10.13031/2013.20488

Hostache, R., Matgen, P., Schumann, G., Puech, C., Hoffmann, L., & Pfister, L. (2009). Water level estimation and reduction of hydraulic model calibration uncertainties using satellite SAR images of floods. *IEEE Transactions on Geoscience and Remote Sensing*, *47*(2), 431–441. https://doi.org/10.1109/TGRS.2008.2008718

McFeeters, S. K. (1996). The use of the normalized difference water index (NDWI) in the delineation of open water features. *International Journal of Remote Sensing*, *17*(7), 1425–1432. https://doi.org/10.1080/01431169608948714

Mohamed, M. A., & Kim, K. E. (2003). *Use of texture filters to improve quality of digital elevation models derived from stereo imagery*. Paper presented at Geoscience and Remote Sensing Symposium, IEEE, Toulouse, France. https://doi.org/10.1109/IGARSS.2003.1293715

Morin, P., Porter, C., Cloutier, M., Howat, I., Noh, M. J., Willis, M., et al. (2016). ArcticDEM; a publically available, high resolution elevation model of the Arctic. EGU General Assembly Conference Abstracts, 18, 8396.

Noh, M. J., & Howat, I. M. (2015). Automated stereo-photogrammetric DEM generation at high latitudes: Surface extraction with TIN-based search-space minimization (SETSM) validation and demonstration over glaciated regions. *GIScience & Remote Sensing*, *52*(2), 198–217. https://doi.org/10.1080/15481603.2015.1008621

Noh, M. J., & Howat, I. M. (2017). The surface extraction from TIN based search-space minimization (SETSM) algorithm. *ISPRS Journal of Photogrammetry and Remote Sensing*, *129*, 55–76. https://doi.org/10.1016/j.isprsjprs.2017.04.019

Nuth, C., & Kääb, A. (2011). Co-registration and bias corrections of satellite elevation data sets for quantifying glacier thickness change. *The Cryosphere*, *5*(1), 271–290. https://doi.org/10.5194/tc-5-271-2011

Ottinger, M., Kuenzer, C., Liu, G., Wang, S., & Dech, S. (2013). Monitoring land cover dynamics in the Yellow River Delta from 1995 to 2010 based on Landsat 5 TM. *Applied Geography*, *44*, 53–68. https://doi.org/10.1016/j.apgeog.2013.07.003

Papa, F., Bala, S. K., Pandey, R. K., Durand, F., Gopalakrishna, V. V., Rahman, A., & Rossow, W. B. (2012). Ganga-Brahmaputra river discharge from Jason-2 radar altimetry: An update to the long-term satellite-derived estimates of continental freshwater forcing flux into the Bay of Bengal. *Journal of Geophysical Research*, *117*, C11021. https://doi.org/10.1029/2012JC008158

Pavelsky, T. M. (2014). Using width-based rating curves from spatially discontinuous satellite imagery to monitor river discharge. *Hydrological Processes*, *28*(6), 3035–3040.

Pavelsky, T. M., Durand, M. T., Andreadis, K. M., Beighley, R. E., Paiva, R. C., Allen, G. H., & Miller, Z. F. (2014). Assessing the potential global extent of SWOT river discharge observations. *Journal of Hydrology*, *519*, 1516–1525. https://doi.org/10.1016/j.jhydrol.2014.08.044

Peterson, B. J. (2002). Increasing river discharge to the Arctic Ocean. *Science*, *298*(5601), 2171–2173. https://doi.org/10.1126/science.1077445

Schumann, G., Hostache, R., Puech, C., Hoffmann, L., Matgen, P., Pappenberger, F., & Pfister, L. (2007). High-resolution 3-D flood information from radar imagery for flood hazard management. *IEEE Transactions on Geoscience and Remote Sensing*, *45*(6), 1715–1725. https://doi.org/10.1109/TGRS.2006.888103

Steele, M., Thomas, D., Rothrock, D., & Martin, S. (1996). A simple model study of the Arctic Ocean freshwater balance, 1979–1985. *Journal of Geophysical Research*, *101*(C9), 20,833–20,848. https://doi.org/10.1029/96JC01686

Tseng, K. H., Shum, C. K., Kim, J. W., Wang, X., Zhu, K., & Cheng, X. (2016). Integrating Landsat imageries and digital elevation models to infer water level change in Hoover dam. *IEEE Journal of Selected Topics in Applied Earth Observations and Remote Sensing*, *9*(4), 1696–1709. https://doi.org/10.1109/JSTARS.2015.2500599

Wessel, P., & Smith, W. H. (1991). Free software helps map and display data. *Eos, Transactions American Geophysical Union*, *72*(41), 441–446. https://doi.org/10.1029/90EO00319

Zhao, D., Cai, Y., Jiang, H., Xu, D., Zhang, W., & An, S. (2011). Estimation of water clarity in Taihu Lake and surrounding rivers using Landsat imagery. *Advances in Water Resources*, *34*(2), 165–173. https://doi.org/10.1016/j.advwatres.2010.08.010

Zhaohui, Z, Prinet, V., & Songde, M. A. (2003). Water body extraction from multi-source satellite images. IEEE Geoscience and Remote Sensing Symposium, IGARSS'03, Proceedings, 6, 3970–3972.